Bi Dendrites Succeed under Challenging Flue Gas Conditions for CO_2RR

*Payal Allawadhi[a], Gavin Mountjoy[b], Rahul Kumar Yadav[a], Ravi Kumar[c], Dibyendu Bhattacharyya[c] and Deepa Khushalani[a]**

[a]Materials Chemistry Group, Department of Chemical Sciences, Tata Institute of Fundamental Research, Mumbai, 400005, India

[b]School of Physics and Astronomy, University of Kent, Canterbury, CT2 7NH, UK

[c]Atomic and Molecular Physics Division, Bhabha Atomic Research Centre, Mumbai, 400085, India

Keywords: Electrochemical CO_2 reduction, Operando XANES, Diluted CO_2, Flue gas, Metallic catalysts

Abstract

The electrochemical reduction of carbon dioxide (ERC) from flue gas is a promising solution to mitigate CO_2 emissions and importantly has the ability for direct industrial application. However, components such as N_2, O_2, SO_x, NO_x, and H_2O in flue gas can hinder ERC efficiency, affecting catalyst stability and selectivity. This study systematically investigates the effect of these flue gas components on a metallic Bi dendrite catalyst. The catalyst shows remarkable stability (over 6 days are observed with constant current generation) surpassing other monometallic Bi catalysts. The active state of the catalyst has been demonstrated with o*perando* XANES analysis which has confirmed the metallic state of bismuth and notably, the catalyst performance remains unaffected despite presence of other flue gas components such as N_2, O_2, SO_x, and NO_x. This research aims to fill a critical gap, demonstrating how flue gas components influence ERC activity and paves a way for future advancements in catalyst optimization.

1. Introduction

It is well known that reliance on fossil fuels has led to significant environmental challenges, including global warming. Among all the greenhouse gases, carbon dioxide (CO_2) has not only been the main largest component but also has been a primary contributor to most of the adverse

effects. For the past several decades, the scientific community has been focusing on various ways to capture, store, and convert CO_2. Of all the routes available, electrochemical CO_2 reduction (ECR) is an easier way that aims to use renewable energy resources to provide simultaneous benefits of capturing and converting CO_2 into useful products such as hydrocarbons, alcohols, aldehydes, and acids.[1-3] This route, in principle, allows ease of CO_2 utilization as, ideally, there is no need for compression, desorption, transportation of the gas and in principle there is direct value creation from the captured CO_2. As such, there has been an almost exponential rise in publications associated with ECR over the last few decades, however, despite these publications amounting to over 2500 as of 2023, the practical applicability of catalysts has not met industrial requirements (**Figure S1**). This is predominantly because more than 95% of the studies that are published annually use solely 100% CO_2 as the reagent. This does not represent real-world scenarios as ultimately, CO_2 from the environment needs to be used, where its concentration is 0.04%. Hence, an additional, consequential step is inserted which involves purification. In order to circumvent this financially costly step, it is, imperative to perform studies using industrially relevant feedstock. The use of gas compositions that mimic flue gas are viable candidates. Flue gas conventionally has a concentration of CO_2 at *ca.* 20%, and this has the potential to enhance the possibility of capturing and converting CO_2 effectively. However, flue gas comprises several other components such as N_2 (50-80 %), O_2 (2-15 %), SO_x (0.01-0.04 %), NO_x (0.01-0.04 %), and water vapors (5-20 %),[4] which can pose several challenges during the ECR process. For instance, well-known ECR catalysts such as Ag-based catalysts,[5, 6] Cu-based catalysts,[7] and Bi-based systems[8, 9] have also been found as active catalysts for N_2 Reduction Reaction (NRR). N_2 is the major component in flue gas, so selectivity towards ECR can become a mitigating issue when using flue gas. Yang *et al.* in 2023 studied the activity of oxide-derived Bi catalyst using flue gas and found that catalyst efficiency towards ERC was reduced by competitive NRR.[10] In addition, another component, O_2, has a thermodynamically favorable reduction potentials (E^o O_2 / H_2O = 1.23 V, E^o O_2 / H_2O_2 = 0.70 V and E^o O_2 / OH^- = 0.40 V *vs*. SHE) relative to CO_2 (E^o CO_2 / $HCOO^-$ = -0.31 V *vs*. SHE), and N_2 (E^o N_2 / NH_4^+) = 0.27 V vs. SHE. This aspect, unfortunately, therefore, makes O_2 relatively more prone to reduction.[11-13] It has also been stated that O_2 and N_2 2p orbitals can undergo back bonding with certain catalysts and this in turn can lead to their facile adsorption and subsequently can reduce the number of active sites.[14] Furthermore, SO_x and NO_x are the minor but corrosive impurities present in flue gas that can undergo hydrolysis in water and can produce acids, which can lead to catalyst instability.[15] Hence, to address all these impediments,

a systematic study to identify the key flue gas component that can affect ERC activity is required.

For ECR, various electrodes such as Cu,[2, 16-18] Pb,[19-21] Pd,[22, 23] Ag,[24, 25] In,[26, 27] Bi,[28, 29] and Sn [30, 31] have been explored. Bi has emerged as a compelling candidate owing to its cost-effectiveness, non-toxicity, and high selectivity towards CO_2 reduction to formate.[28, 29, 32] There are various forms of bismuth that have been explored other than metallic bismuth such as bismuth MOFs[33, 34] and various derivatives including bismuth oxides and sulfides.[35, 36] However, these catalysts can face issues as these compounds are easily polarisable. As such, electrochemical response at varying potentials can lead to both structural and chemical unstability. In a report by Cao *et al.*, Bi-MOF underwent a transformation to ultrathin bismuthenes just by electrochemical treatment at low potentials.[37] Lamagni *et al.* reported a Bi-based MOF that was structurally distorted at reducing potentials during ECR.[33] Yao *et al.* found that HCO_3^- electrolyte cleaved the Bi-O bond entirely in a bismuth carboxylate MOF.[38] Zhu *et al.* had to explore coating methods to address the instability that occurred due to the polarisable nature of oxide and sulfide interfaces.[39]

To overcome the challenges discussed above, metallic bismuth has been chosen as the catalyst due to its expected intrinsic stability. This makes it a particularly strong candidate for applications involving flue gas, where catalysts must withstand extremely harsh conditions over extended periods. The selection of bismuth is based on the assumption that its metallic form will offer greater robustness and longevity compared to other potential materials.

Historically, bismuth catalysts have been tested only in 100% CO_2, and to the best of our knowledge, no comprehensive studies on the effects of individual flue gas components or the long-term durability of these catalysts in flue gas environments is available. This study aims to address this lacuna and as such the work here details the individual effect of each flue gas component involving N_2, O_2, SO_x, and NO_x on metallic Bi catalyst, along with all the components in unison. The catalyst has been electrochemically deposited using a unique dynamic hydrogen bubble template method (DHBT). In this method, simultaneous *in situ* generation of hydrogen bubbles (*via* water reduction) occurs and these act as templates and ensure the concurrent deposition of high surface area Bi, which interestingly has a preferential ordering of high index planes relative to the (003) plane. The entire deposition process occurs rapidly in a few seconds. Moreover, *operando* XANES has been employed to confirm the zero valent nature of Bi during the ECR process and also the effect of flue gas components such as N_2, O_2, SO_x, and NO_x individually on the ECR activity of the catalyst has been shown.

Importantly, the long-term stability of the catalyst (> 30 hours) in the presence of simulated flue gas has been detailed.

2. Results and Discussions

2.1. Structural Characterization of Bismuth Catalyst

Bi was electrochemically deposited on a substrate using an electrolyte consisting of bismuth nitrate dissolved in nitric acid and by applying a constant current density. Initially, three different catalysts were deposited: (a) For Bi(A) sample, Cu foil was the working electrode on which 3 A/cm^2 was provided for 5 sec., (b) Bi(B) sample, Cu foil was the working electrode on which 3 A/cm^2 was provided for 10 sec., and (c) Bi(C) sample where Pt foil was the working electrode on which 3 A/cm^2 was provided for 5 sec. The schematic for deposition is shown in **Figure S2**. Upon evaluation of these three samples, it was observed all three have dendritic morphology, however, it was found that Bi(A) had the thinner dendrites as compared to Bi(B) and Bi(C). Full electrochemical evaluation of these materials was done using 100% CO_2 and to be succinct, it was found that Bi(A) had better electrochemical behavior for ERC at both higher voltage of -0.95 V and low voltage of -0.65 V as compared to Bi(B) and Bi(C). It needs to be noted that despite the morphology of the three samples of Bi being very similar there was an important distinction – in that the crystallographic orientation and the planes that are exposed are different. It has been previously shown, through DFT studies, that the relative ratio of (012) plane with respect to (003) plane can significantly help in stabilizing *OCOH – an intermediate that favours the formation of formate.[40] This ratio, for our samples has been measured using XRD data, and the values are compiled in **Section B, Table S-B2.** From this, it is found that Bi(A) and Bi(C) have 1.5 times higher ratio as compared to Bi(B), however in case of Bi(C) another factor participates *i.e*. the substrate is platinum, even though suppression of the HER occurs with dendritic Bi, the amount of H_2 produced at Pt become very pronounced which is not desirable since CO_2RR is the target reaction. Hence, the activity of Bi(A) was found to be higher as compared to Bi(B) and Bi(C). The details of all the measurements have been provided in **Sections A** and **B** of Supplementary Information. Considering this aspect, all the subsequent studies to evaluate the activity in the presence of flue gas components have been solely done on Bi(A).

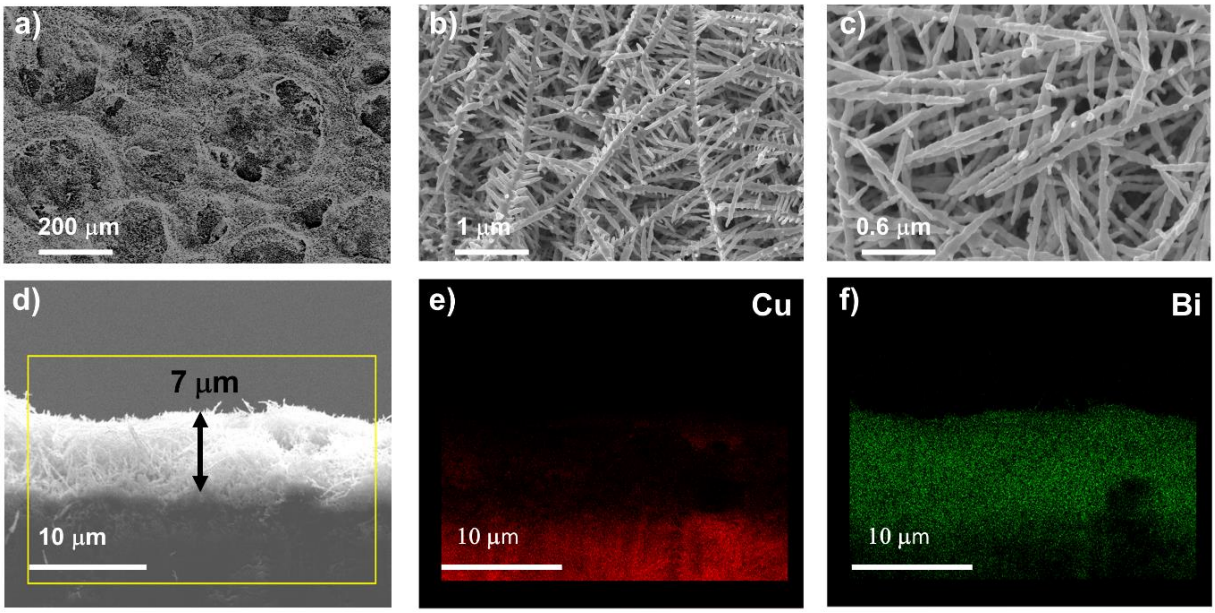

Figure 1. (a-c) SEM images of the top view **(d-f)** EDX mapping of the cross-section of Bi(A)

Figure 1 (a-c) shows SEM images of Bi(A) which suggests that the sample consists of dendritic morphology (width of *ca*. 100 nm) that is distributed evenly and there is minimal exposure of underlying Cu substrate. The morphology and positioning of dendrites is such there are spaces present which can easily allow the electrolyte to permeate and access the active sites. Cross-sectional EDX imaging shows that a 7 µm layer of Bi is present, which is further confirmed by EDX mapping, **Figure 1 (d-f)**. EDX analysis of the catalyst shows the presence of Bi and Cu and EDX mapping of the top view further confirms that Bi is distributed evenly, **Figure S3. Figure 2** shows X-ray diffraction (XRD) and TEM images of the catalyst and solely Bi is found to be present. Underlying Cu substrate can also be detected via XRD. Notably, the specific DHBT method detailed for Bi deposition has enabled the synthesis of a sample with significantly enhanced intensity of high-index planes such as (012), (110), and (104) relative to the (003) plane. Based on work detailed by Koh and co-workers, this orientation is expected to provide sustainable performance of the catalyst.[40] The selected area electron diffraction (SAED) image confirmed the crystallinity and phase purity of the Bi dendrites and the electron diffraction data is in agreement with the XRD data.

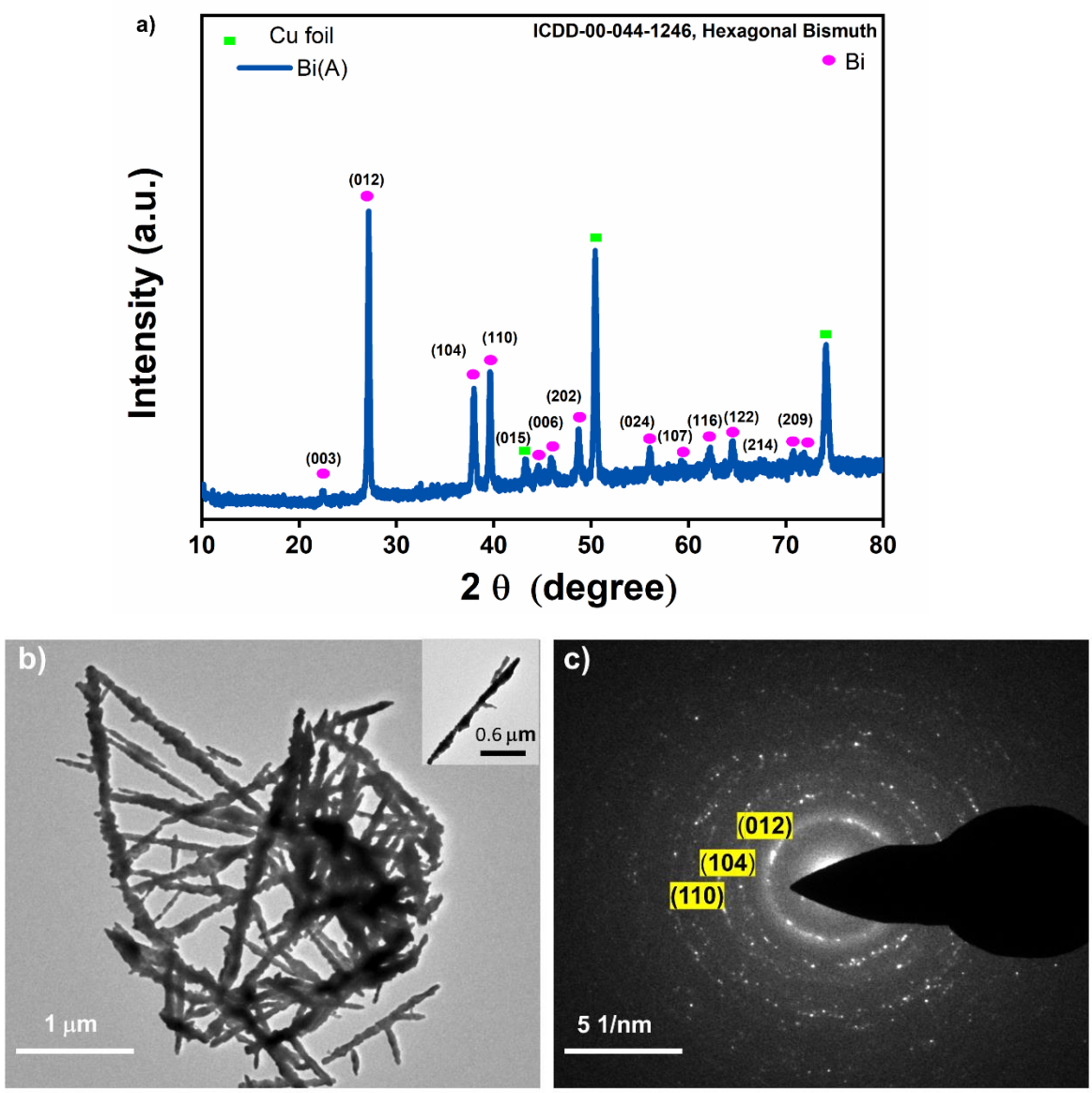

Figure 2 (a) XRD pattern of Bi(A) **(b)** TEM image of a large number of dendrites of Bi(A) and **(c)** their SAED image.

2.2. Electrochemical evaluation of Bi(A) in the presence of pure CO_2

Firstly, the performance of Bi(A) was measured in the presence of 100% CO_2 to obtain baseline values for the activity of the catalyst towards ERC. Linear Sweep Voltammetry data (LSV) for Bi(A) is shown in **Figure 3a** and compared with pure Cu substrate. There is a feature at 881 mV which is observed in the case of Bi(A) and it corresponds to the reduction of bismuth, see section 2.3 for further confirmation below. **Figure 3b** shows chronoamperometry plots for Bi(A) and Cu at three different voltages. It can be seen that Bi(A) shows impressive stability with constant current at even high voltage of -1.5 V. Both LSV and chronoamperometry

measurements suggest higher reduction current values in the case of Cu as compared to Bi(A). Impedance measurements for Bi(A) are shown in **Figure 3c.** The curve in the high-frequency region represents the charge transfer process during ECR, and the sloping line at low frequencies represents the reactant diffusion process during ECR.[41] The charge transfer resistance value obtained from the modelled equivalent circuit is found to be lower than the reported bismuth dendrites where the values have ranged from 19-25 Ω.[41-43] This is believed to be a direct consequence of the facile manner in which DHBT deposition technique allows for a well formed electrical contact between the catalyst and the underlying electrode. From the double layer capacitance value obtained, the electrochemical surface area (ECSA) for Bi(A) was found to be 61 cm^2 (value of specific capacitance of bismuth used was 28 $\mu F/cm^2$).[44] Following the chronoamperometry experiments, reduction products were analyzed by NMR and Gas Chromatography. For comparison, the data has been shown for bare Cu substrate, in **Figure 3d**. In the case of Bi(A), formate and methane are observed as CO_2 reduction products, and H_2 is obtained as a result of water reduction. However, in the case of Cu, formate and CO are observed as the CO_2 reduction products. The production of all the products increases with an increase in voltage, **Figure 3e**. It is important to note that CO was not detected in the experiments with Bi (as compared to data from the sole use of Cu as the substrate). This is advantageous as CO is considered to not be a highly desirable product since it requires additional costs for processing into other chemicals using the Fischer Tropsch synthetic pathway.[45] Moreover for Bi(A), methane production is also observed which in not seen in the case of Cu, under similar conditions. It needs to be noted methane formation is an 8 electron process and no other carbon based products were observed other than methane and formate. At each voltage, Bi(A) produced more formate and less hydrogen when compared to the Cu substrate which suggests that the catalyst is more active towards ECR. In the case of Cu, at all the voltages < 20% faradaic efficiency value for formate was obtained, whereas in the case of Bi(A), it reaches *ca.* 70 % faradaic efficiency at -0.65 V, **Figure 3f.** From this data, it can be inferred that copper is a less selective catalyst for formate production from ECR. The higher current values obtained in the case of Cu during electrochemical measurements can therefore be ascribed to predominantly HER and not due to formate production.

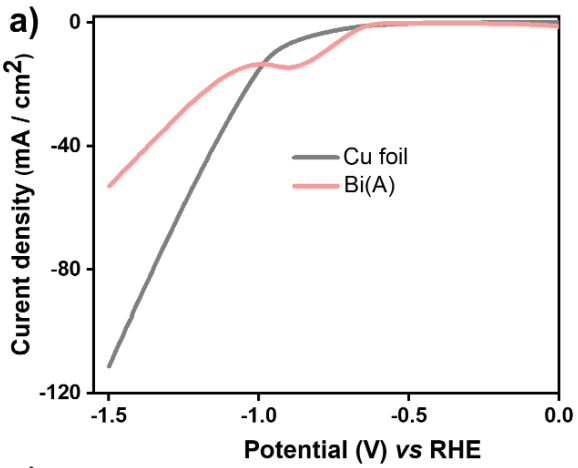

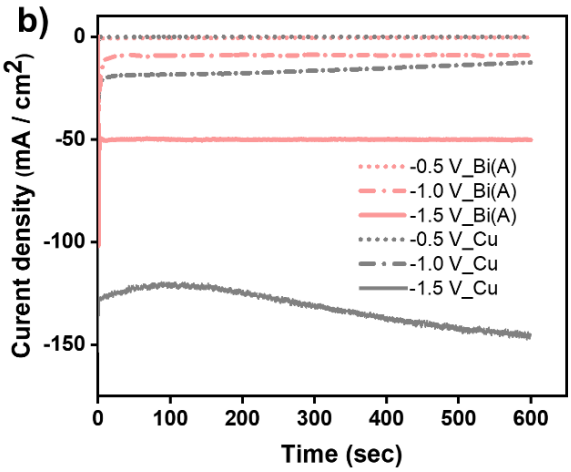

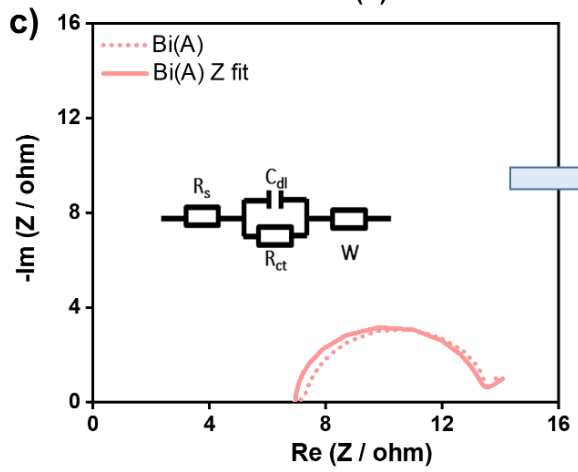

Solution Resistance, R_s (Ω)	**6.9**
Capacitance, C_{dl} (F)	**1.7 X10^{-3}**
Charge transfer Resistance, R_{ct} (Ω)	**6.1**
Warburg Resistance, W (Ω s$^{-1/2}$)	**0.7**

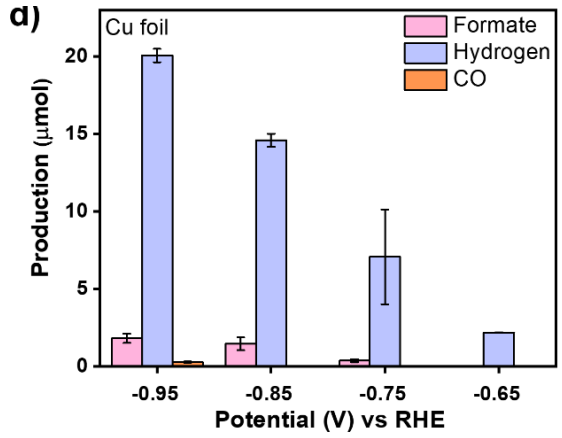

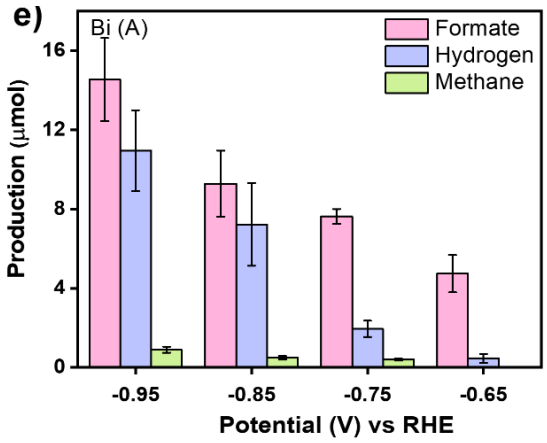

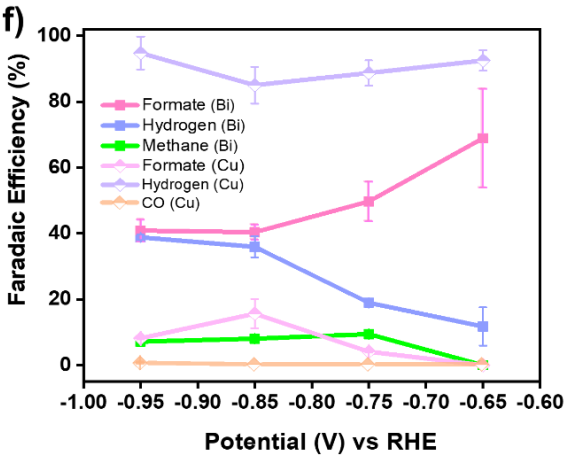

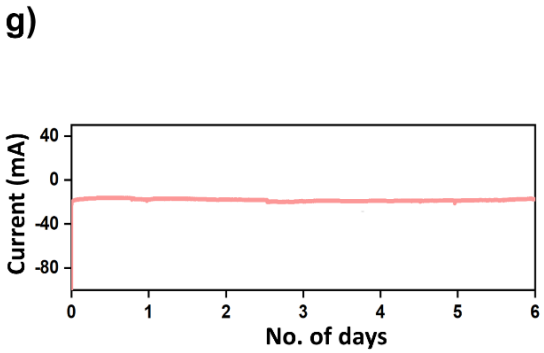

Figure 3 (a) Linear Sweep Voltammetry plot for Bi(A) and Cu foil at a scan rate of 20 mVs^{-1} **(b)** Constant potential electrolysis at -0.5 V, -1.0 V, and -1.5 V for Bi(A) and Cu. **(c)** Impedance measurements for the Bi(A) at -0.75 V *vs* RHE. Production of various reduction products in cases of the **(d)** Cu and **(e)** Bi(A) respectively at different voltages. Faradaic Efficiency values of various reduction products in the case of the **(f)** Bi(A) and Cu **(g)** Chronoamperometry data at -1 V *vs* RHE for Bi(A) done for a prolonged period of 6 days. Counter Electrode - Platinum, Reference Electrode – Ag / AgCl (sat. KCl) and Electrolyte: 1 M $KHCO_3$

In order to ensure that use of a metallic catalyst was stable, chronoamperometry measurements were carried over a continuous exposure to CO_2 at -1 V for 6 days **Figure 3g.** It is important to note that there was negligible variation in the current and the current loss after 6 days was less than 7%.

2.3 *Operando* evaluation of Bi(A) during ERC

Before proceeding to flue gas studies, it is important to understand the nature of the catalyst formed. Moreover, considering the high stability of Bi(A) based on chronoamperometry studies, an evaluation of the exact chemical nature of Bi was undertaken using *operando* X-ray Absorption Near Edge Structure spectroscopy. XANES is most commonly used to study the oxidation state and coordination geometry and Bi L_3-edge XANES is a very useful probe to understand the state of Bi in the catalyst under redox conditions. The setup used for XANES is shown in **Figure S4** and details of the experiment are given in the experimental section below. The XANES spectra of the catalyst at Bi L_3-edge was recorded without any bias and under *operando* conditions when -0.75 V was applied. The edge positions obtained were compared with the edge positions obtained in *ex-situ* conditions for three different references of Bi-based compounds having different oxidation states of Bi. XANES results show that when -0.75 V is applied to the catalyst, it is found that Bi is reduced to a 0 valent state, **Figure 4a** which is suggested by the considerable 4.5 eV and 6.5 eV shift in the binding energy of the absorption edge relative to Bi^{3+} and Bi^{5+} reference respectively. However, before the application of the voltage, its edge position value lies in between the values obtained for Bi^0 and Bi^{3+} case. To confirm this even further, the experimentally obtained data was compared with a computed edge position (obtained after a linear combination of the edge position of Bi^0 and Bi^{3+}). The similarities suggests that the catalyst was initially partially oxidized, **Figure 4b**. In literature, efforts have been made to discern the actual catalytic site in the case of bismuth-based catalysts

during ERC through *in-situ* and *operando* measurements.[46-48] However, there are no reports available for solely Bi catalysts to know the actual catalytic state during reduction through operando XANES. Hence, for the first time, it can be unequivocally shown that Bi does form an oxide phase, as before the application of voltage, the catalyst is partially oxidized, however, during catalysis, Bi is present in the metallic state. Since metals are known to have high intrinsic stability hence, this is purported to be the reason that the Bi(A) catalyst shows extraordinary stability of upwards of 6 days.

It needs to be highlighted that for most of the previously reported monometallic Bi catalysts, the stability during ERC has only been shown upto 30 hours, data shown in **Figure S5a**, but this study has been able to show the persistence of stable current density value for up to 6 days, and moreover the comparison of faradaic efficiency of this catalyst compared to the host of other Bi based systems is shown in **Figure S5**. It can be seen that the sustainable performance of catalyst Bi(A) is substantially higher (even at a high voltage of - 0.95V) as compared to other reported systems. From this promising data, Bi(A) was therefore exposed for further evaluation. Following are details of the measurements done on Bi(A) using initially individual components of flue gas and then in presence of simulated flue gas.

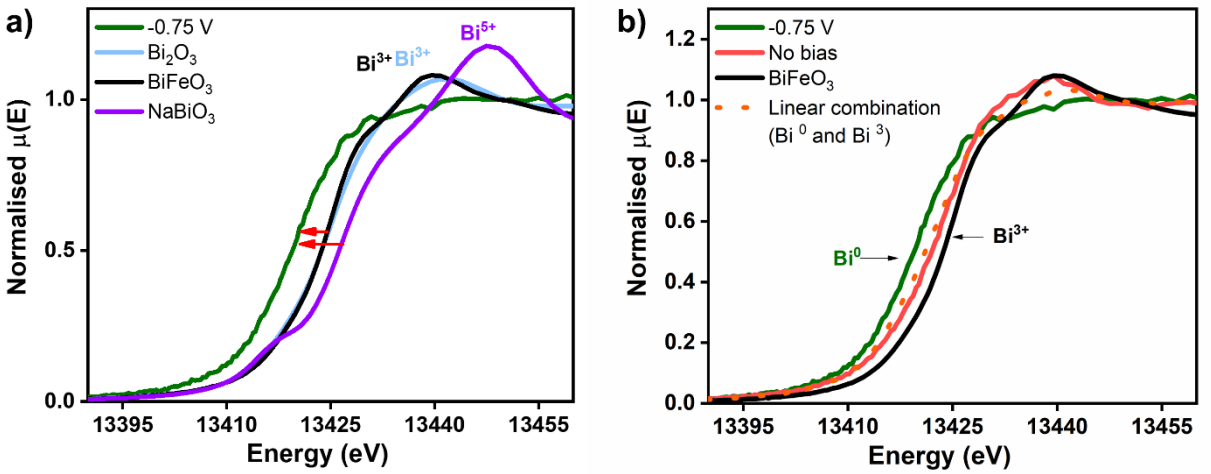

Figure 4 (a) Bi L_3-edge XANES spectra of reference compounds Bi_2O_3, $BiFeO_3$, $NaBiFeO_3$ with Bi oxidation states of +3, +3 and +5 respectively done under *ex-situ* conditions and Bi(A) at -0.75 V *vs* RHE done under *operando* conditions in fluorescence mode **(b)** Bi L_3-edge XANES spectra of Bi(A) without bias (orange solid plot) which matches with the spectra obtained by a linear combination of Bi^0 and Bi^{3+} (orange dotted plot).

2.4. Electrocatalysis of Bi(A) in the presence of flue gas components - N_2 and O_2

To investigate the interference of N_2 and O_2, CO_2 was diluted to 50% with these gases individually, and constant potential electrolysis was done at 3 voltages (-0.75, -0.85 and -0.95V) and the reduction products were analyzed, **Figure S6 and S7.** It was found that whether the reagent gas was diluted with either N_2 or O_2, in both cases formate, hydrogen and methane were forming. However in case O_2 as the diluting gas, other than methane and formate, a trace amount of CO was also obtained as an additional reduction product**.** Moreover, there were no adverse effects on the current density observed with addition of either N_2 or O_2, and production of the products was always consistently higher at higher voltages.

All the products measured and their selectivity are shown in **Figure 5.** It can be observed that similar trend of formate FE was observed at all voltages regardless of the presence of N_2 or O_2**.** There was however a marginal reduction in formate selectivity at higher voltages *c.a.* -0.95 V relative to the baseline results obtained in the case of pure CO_2**.** This can solely be ascribed to the dilution effect and not due to interference of N_2 or O_2 on the active site. To understand this aspect further, CO_2 was sequentially diluted with N_2 and O_2 in different percentages - 75%, 50% and 25%, **Figure 5 (d-g)**. It is observed that, with a linear decrease in the percentage of CO_2, despite either N_2 or O_2 being present, a linear trend in the reduction of formate production was observed (Slope - 0.93 and 0.97 respectively), which suggested that the active sites on Bi(A) were not being occupied by either N_2 or O_2 and as such presence of these additional additives did not affect selectivity towards CO_2. Detailed quantification of all products obtained is shown in **Figure S8.**

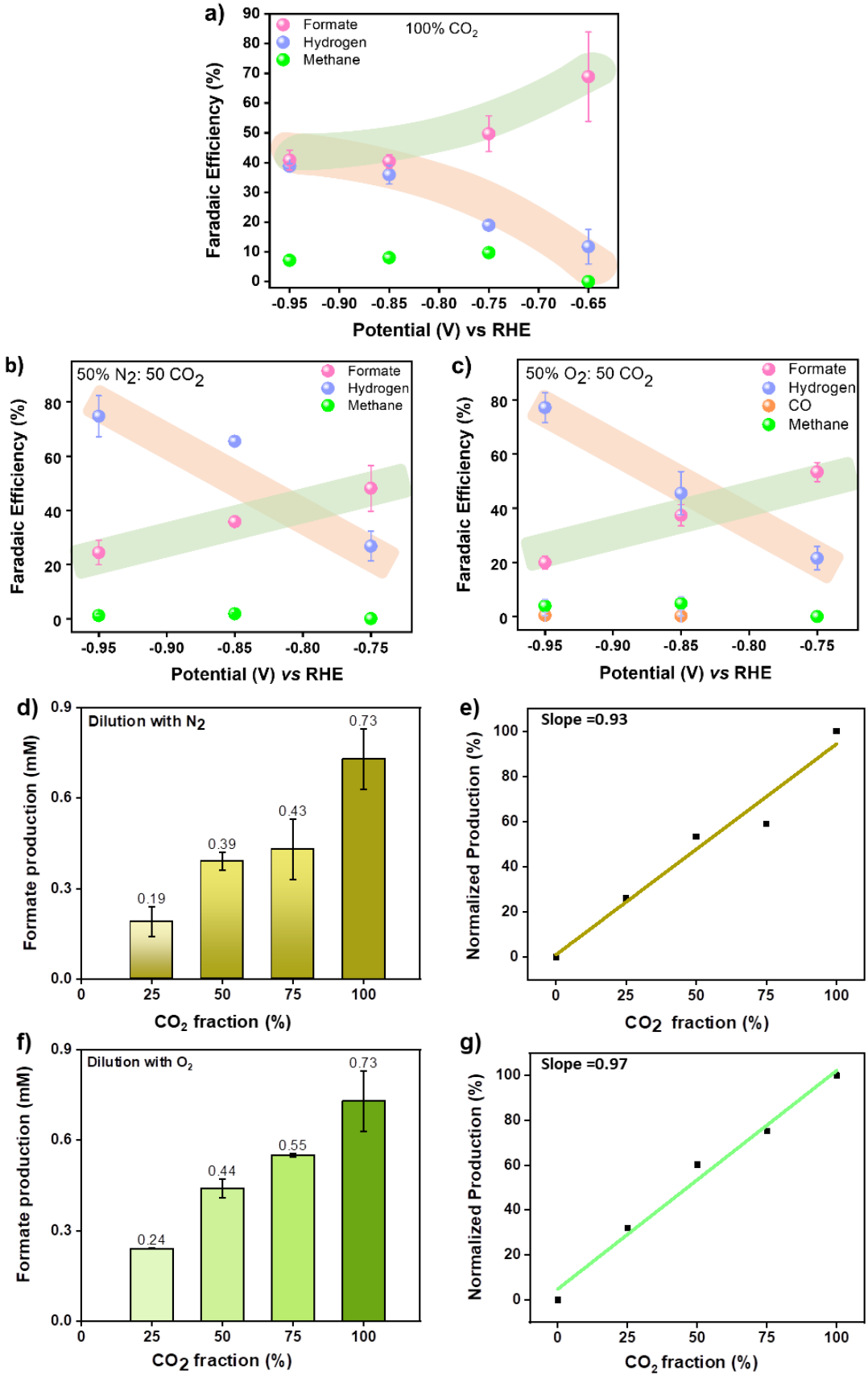
a)
Formate
Hydrogen
Methane
100% CO2
Faradaic Efficiency (%)
Potential (V) vs RHE
b)
50% N2: 50 CO2
Formate
Hydrogen
Methane
Faradaic Efficiency (%)
Potential (V) vs RHE
c)
50% O2: 50 CO2
Formate
Hydrogen
CO
Methane
Faradaic Efficiency (%)
Potential (V) vs RHE
d)
Dilution with N2
0.19
0.39
0.43
0.73
Formate production (mM)
CO2 fraction (%)
e)
Slope =0.93
Normalized Production (%)
CO2 fraction (%)
f)
Dilution with O2
0.24
0.44
0.55
0.73
Formate production (mM)
CO2 fraction (%)
g)
Slope =0.97
Normalized Production (%)
CO2 fraction (%)

Figure 5. Faradaic Efficiency plot for various reduction products obtained for Bi(A) when CO_2 electrolysis is done at different voltages **(a)** with pure 100% CO_2, **(b)** with 50% CO_2 diluted with nitrogen **(c)** with 50% CO_2 diluted with oxygen. Production of formate with different percentages of CO_2 - 75%, 50%, 25% when diluted with **(d)** nitrogen and **(e)** linear fit of normalized production values obtained from corresponding CO_2 fraction (%). Production of formate with different percentages of CO_2 - 75%, 50%, 25% when diluted with **(f)** oxygen and **(g)** linear fit of normalized production values obtained from corresponding CO_2 fraction (%)

2.5. Effect of activity of Bi(A) in the presence of all flue gas components

In order to understand the effect of SO_x and NO_x, the activity of the catalyst was now comprehensively checked in the presence of fully simulated flue gas which included 15 % CO_2, 0.020 % SO_x, 0.015 % NO_x, and balance N_2. During flue gas measurements, only NMR studies were performed to evaluate product formation (Gas Chromatography measurements could not be performed due to the corrosive nature of flue gas). The activity obtained was now compared with the activity obtained in the presence of a control experiment which included the reagent gas bearing a composition of 15% CO_2 and 85% N_2. From the LSV and chronoamperometry plot, **Figure 6,** it can be inferred that the onset potential to reach 1 mA/cm^2 current density, was 615 mV for control gas while for flue gas it was 588 mV. Moreover, there was *insignificant* alteration in current density during a chronoamperometry experiment, **Figure 6b**, observed in both cases, which suggested that SO_x and NO_x were not affecting the activity of the catalyst. These plots suggested similar kinetics for the ECR in both cases. It needs to be noted that reduction peak observed in LSV at *ca*. 881 mV (which has been ascribed to the reduction of Bi^{3+} based on XANES) was more pronounced when flue gas was used. This can be rationalized by the aspect that, before intiating any electrochemical experiment, the electrolyte is purged with the reagent gas for *ca.* 30 minutes. As flue gas was used, the additional oxidation of the catalyst can be ascribed due to the presence of SO_x and NO_x.[15] However, as has already been shown, this oxidized catalyst is not the active state and the catalyst forms a 0 valent state when sufficient potential is applied. Interestingly, there is not much change in the production and selectivity of formate as observed in **Figure 6 (c,d)** and in fact there is an augmentation in the presence of flue gas when compared to the control reagent gas**.** This suggests the activity of the catalyst is retained even in the presence of SO_x and NO_x and the reactive catalytic sites appear to be fully accessible. Further, long-term stability was checked for Bi(A) for upwards of 30

hours and there was no decay in the presence of flue gas, **Figure 6e.** The characterization of the Bi(A) catalyst (after 30 hours of electrochemical study) was done by SEM and EDX. **Figure S9** shows that there is no considerable effect on the morphology and the EDX showed solely elements corresponding to either electrolyte or Bi. There was an absence of any other elements corresponding to flue gas (sulphur or nitrogen) which suggests that there is no chemisorption of these occurring on the surface of Bi. It also needs to be noted that there were no measurable pH changes observed of the electrolyte during these prolonged experiments. This observation implies that a possible competing NRR reaction is not occurring where ideally NH_3 should be a product. In order to put this work in perspective with other similar literature reports, **Table 1** details a comparison between our work and two other reports that have also used Bi-based catalysts for evaluation of CO_2RR using some selected components of flue gas. It can be observed that the work presented here has been done with all components and more importantly Bi(A) shows better stability in presence of all the components of flue gas for a more prolonged period.

In summary, Bi(A) does not show any deleterious effects of using a reagent gas consisting of 15 % CO_2, 0.020 % SO_x, 0.015 % NO_x, and balance being N_2. There appear to be negligible effects of the additives to ECR behavior of the Bi dendrites and the catalyst continues to be stable despite presence of the reactive gases. The findings suggest that Bi's performance remains largely unaffected by these impurities, demonstrating its potential for practical applications in CO_2 conversion technologies.

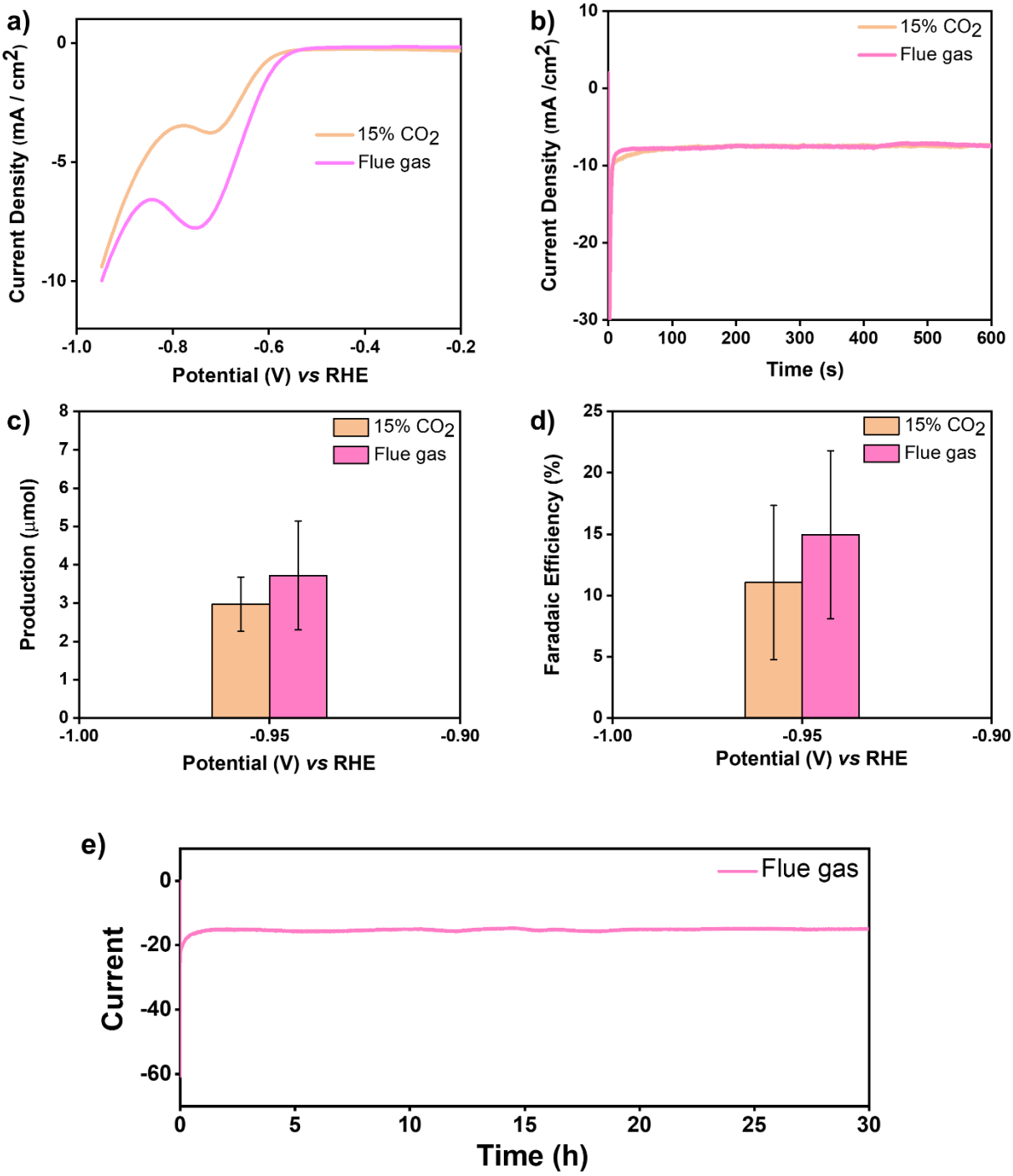

Figure 6 (a) Linear Sweep Voltammetry curves for Bi(A) at a scan rate of 20 mVs^{-1} when the potential is swept from -0.2 V to -0.95 V *vs* RHE **(b)** Chronoamperometry plot at -0.95 V *vs* RHE **(c)** Formate Production and **(d)** Faradaic Efficiency plots at -0.95 V for Bi(A) in the presence of flue gas and in presence of 15% CO_2 balanced with nitrogen, **(e)** Long term stability (chronoamperometry experiment) for the Bi(A) in the presence of flue gas at -1 V.

Table 1. Comparison of stability obtained in this work in the presence of flue gas components with reported single metal-based bismuth catalyst.

Material	Components	Stability (hrs)	Reference
Bi_2O_3	SO_x, NO_x (<1 %) balance N_2	20	[49]
Oxide derived-Bi	15% CO_2, trace amount of O_2 and SO_2, balance N_2	12	[10]
Bi(A)	***15% CO_2, SO_x, (0.02 %), NO_x (0.015 %), balance N_2***	***30***	***This work***

3. Conclusions

This study highlights the performance of Bi dendrite based catalyst in the presence of various flue gas components. The baseline values for the activity of the catalyst in 100% CO_2 showed a selectivity of *ca*. 70 % for formation of formate at a low potential of -0.65 V, and further, the catalyst was able to survive under a relatively harsh potential value of -1 V for 6 days. Formate, an ECR product of bismuth under aqueous conditions, has its advantages as it has been demonstrated to have high energy storage value, a precursor for producing chemicals, hydrogen storage material, and is a promising feedstock for fuel cell applications.[28]

Further, operando XANES have been used to probe the actual catalytic state of Bi, suggesting that metallic Bi is responsible for the reduction. The key findings under flue gas conditions suggested that the Bi catalyst remains selective towards CO_2 gas despite the presence of other competitive flue gas components such as N_2, O_2, SO_x, and NO_x. Further, this study has shown upwards of 30 hours of stability in the presence of flue gas. This study shows the impact of each flue gas components on the activity of bismuth catalyst and provides a roadmap to apply to other catalysts to study the impact of flue gas components.

4. Experimental Section

4.1. Preparation of Bi electrode

Before deposition on the Cu substrate, the foil was pre-treated with 1M HNO_3 for 5 sec followed by polishing to remove the oxide layer on its surface. The platinum mesh was sonicated for half an hour in 1 M HNO_3 solution. Bi dendrites were electrochemically deposited onto the pre-cleaned substrates, with the deposition solution prepared as follows. 4.18 g of $Bi(NO_3)_3$ was dissolved in 1.5 mM, 100 ml nitric acid solution. For deposition, 15 ml of this solution served as the electrolyte in a two-electrode setup, with Cu (1 cm^2) substrate served as the cathode and a platinum mesh as the anode. A current density of 3 A / cm^2 was passed for 5 sec to deposit on the Cu and the electrode was named as Bi(A), and when deposition time was increased to 10 sec keeping other parametrs constant, it was named as Bi(B). When deposition was done by applying 3 A /cm^2 for 5 sec on Pt substrate , then the electrode was named as Bi(C). After deposition the as-synthesized catalysts were washed gently with distilled water 4-5 times.

4.2. Characterization

4.2.1. Powder X-ray diffraction (XRD)

XRD data acquisition was done under ambient conditions using a Rigaku smart lab X-ray diffractometer with power 9 kW using monochromatic Cu Kα (λ = 0.1547 nm) radiation. The data was acquired for a half-hour in 2Θ range of 5° to 80°.

4.2.2. SEM, TEM and EDX

Measurements were done on Zeiss FESEM Ultra Plus. TEM measurements were done using the Technai T20 TEM.

4.3. Electrochemical measurements

For electrochemical measurements, a three-electrode setup was employed containing working, reference, and counter electrodes. A platinum foil was used as a counter electrode and Ag / AgCl (sat. KCl) was used as the reference electrode. For all the studies, 1 M $KHCO_3$ was used as an electrolyte. All electrochemical experiments have been done under ice bath conditions

except for long-term stability experiments which are done at room temperature. Before the application of voltage, the electrolyte was saturated with the CO_2 gas (diluted or 100% CO_2) and during the experiment, the purging of the gas was continued. The outlet of the electrochemical cell was connected to a container, where all the gaseous products along with CO_2 were collected.

4.3.1 Operando XANES measurements

The XAS measurements have been carried out at the Energy-Scanning EXAFS beamline (BL-9) at the Indus-2 Synchrotron Source (2.5 GeV, 100 mA) at Raja Ramanna Centre for Advanced Technology (RRCAT), Indore, India. Electrochemical parameters were the same as before except the deposition of Bi was done on carbon paper which acted as the working electrode. A special electrochemical cell was used for these measurements in which there is a window where this catalyst is pasted with the help of Kapton tape which is conducting and also transparent to X-rays and also does not allow the electrolyte to come out from the cell.[50] The reason for this special cell is that the X-rays can incident on the catalyst from one side and on the other side it faces the electrolyte. The porous nature of carbon paper allows the electrolyte to access most of the bismuth. Hence, the XANES can be acquired simultaneously while electrocatalysis is undergoing on it.

4.4. Analysis of products

4.4.1. Liquid product analysis

After electrolysis for 10 min, ^{1}H NMR (Bruker 800 MHz spectrometer) was acquired for the aliquot made from 540 μL of reaction mixture mixed with 60 μL of trimethylsilyl propanoic acid in D_2O (TSP, 1 mM) which is taken as a reference. Water suppression was performed to suppress the excess amount of water in the electrolyte.

4.4.2. Gaseous product analysis

Gaseous products were analyzed by micro-GC**.** After the reaction of 10 min, the gaseous sample was injected into GC, which was collected in the container and also another sample was injected from the headspace of the electrochemical cell which still contains the reaction products. The addition of moles produced in both containers for a particular gas represents the total production

for that gas. Traces products like methane and CO were analyzed by directly injecting few microlitres of the gaseous sample from the the continuously flowing stream containing CO_2 and these products.

Supporting Information

Supporting Information is available from the Wiley Online Library or from the author.

Acknowledgements

BB Chandanshive is acknowledged for general laboratory assistance. We thank Rudheer D. Bapat, Manish Garg, and Bhagyashree A. Chalke for their assistance in EM measurements. Vilas J. Mhatre is recognized for XRD support, while Mamata Joshi and Manoj Naik are appreciated for their help with NMR. Sachin Temkar is acknowledged for technical assistance. Department of Atomic Energy, India is gratefully acknowledged for funding of this work through Plan No. 19P0147.

Received: ((will be filled in by the editorial staff))
Revised: ((will be filled in by the editorial staff))
Published online: ((will be filled in by the editorial staff))

5. References

[1] M. Y. Liu, Y. S. Wang, W. Deng, Z. H. Wen, *Prog. Chem.* **2018**, *30*, 398-409.

[2] S. Nitopi, E. Bertheussen, S. B. Scott, X. Y. Liu, A. K. Engstfeld, S. Horch, B. Seger, I. E. L. Stephens, K. Chan, C. Hahn, J. K. Norskov, T. F. Jaramillo, I. Chorkendorff, *Chem. Rev.* **2019**, *119*, 7610-7672.

[3] S. Garg, M. R. Li, A. Z. Weber, L. Ge, L. Y. Li, V. Rudolph, G. X. Wang, T. E. Rufford, *J. Mater. Chem. A* **2020**, *8*, 1511-1544.

[4] S. R. Rachael J Barla, Suresh Gupta, *Waste and Biodiesel*, **2022**, 191-215.

[5] W. Y. Li, K. Li, Y. X. Ye, S. B. Zhang, Y. Y. Liu, G. Z. Wang, C. H. Liang, H. M. Zhang, H. J. Zhao, *ChemComm.* **2021**, *4*, 10.

[6] Y. H. Li, H. J. Yu, Z. Q. Wang, S. L. Liu, Y. Xu, X. N. Li, L. Wang, H. J. Wang, *ChemComm.* **2019**, *55*, 14745-14748.

[7] W. J. Zang, T. Yang, H. Y. Zou, S. B. Xi, H. Zhang, X. M. Liu, Z. K. Kou, Y. H. Du, Y. P. Feng, L. Shen, L. L. Duan, J. Wang, S. J. Pennycook, *ACS Catal.* **2019**, *9*, 10166-10173.

[8] L. Q. Li, C. Tang, B. Q. Xia, H. Y. Jin, Y. Zheng, S. Z. Qiao, *ACS Catal.* **2019**, *9*, 2902-2908.

[9] B. Chang, Q. Liu, N. H. Chen, Y. C. Yang, *Chemcatchem* **2019**, *11*, 1884-1888.

[10] F. Q. Yang, C. H. Liang, W. Z. Zhou, W. D. Zhao, P. F. Li, Z. Y. Hua, H. M. Yu, S. X. Chen, S. G. Deng, J. Li, Y. M. Lam, J. Wang, *Small* **2023**, *19*, 2300417.

[11] S. Chu, R. T. Rashid, Y. Y. Pan, X. T. Wang, H. Y. Zhang, R. Xiao, *J. CO_2 Util.* **2022**, *60*, 101993.

[12] Z. Jiang, T. Zhang, A. M. Rappe, *J. Phys. Chem. C* **2023**, *127*, 40 19879-19885.

[13] D. J. Deng, S. Q. Wu, H. A. Li, H. M. Li, L. Xu, *Small* **2023**, *19*, 2205469.

[14] Q. Hao, C. W. Liu, G. H. Jia, Y. Wang, H. Arandiyan, W. Wei, B. J. Ni, *Mater.Horiz.* **2020**, *7*, 1014-1029.

[15] U. Legrand, U. P. Apfel, D. C. Boffito, J. R. Tavares, *J. CO_2 Util.* **2020**, *42*, 101315.

[16] A. R. Woldu, Z. L. Huang, P. X. Zhao, L. S. Hu, D. Astruc, *Coord. Chem. Rev.* **2022**, *454*, 214340.

[17] M. S. Yesupatham, B. Honnappa, N. Agamendran, S. Y. Kumar, G. Chellasamy, S. Govindaraju, K. Y. S. Yun, N. C. S. Selvam, A. Maruthapillai, W. Li, K. Sekar, *Adv. Sustain. Syst.* **2024**, *8*, 2300549.

[18] B. Rhimi, M. Zhou, Z. X. Yan, X. Y. Cai, Z. F. Jiang, *Nanomicro Lett.* **2024**, *16*, 64

[19] C. Y. Jiang, S. J. Zeng, J. Q. Feng, G. L. Li, B. Hai, K. L. Peng, X. P. Zhang, *J. Mater. Chem. A* **2024**, *12*, 14809-14815.

[20] H. Wang, J. Y. Zhao, Q. Q. Yang, J. C. Wu, X. Y. Zhang, H. Y. Yuan, X. L. Xu, J. J. He, Q. Niu, P. F. Liu, H. G. Yang, *J. Mater. Chem. A* **2024**, *12*, 21406-21411.

[21] Y. R. Xu, X. Liu, M. H. Jiang, B. C. Chi, Y. Lu, J. Guo, Z. M. Wang, S. P. Cui, *J. Colloid Interface Sci.* **2024**, *665*, 365-375.

[22] T. W. Jiang, K. Jiang, W. B. Cai, *J. Mater. Chem. A* **2024**, *12*, 21515-21530.

[23] H. X. Zhao, X. W. Yang, Y. N. Duan, Z. R. Shen, *ChemCatchem* **2024**, *16*, e202301295

[24] A. Conte, M. Baron, S. Bonacchi, S. Antonello, A. Aliprandi, *Nanoscale* **2023**, *15*, 3693-3703.
[25] F. Mattarozzi, N. Visser, J. W. de Rijk, P. Ngene, P. de Jongh, *Eur. J. Inorg. Chem.* **2022**, *2022*, e202200365.
[26] S. M. Li, X. Y. Lu, S. Q. Zhao, M. Ceccato, X. M. Hu, A. Roldan, M. Liu, K. Daasbjerg, *ACS Catal.* **2022**, *12*, 7386-7395.
[27] W. B. Wu, Y. Tong, P. Z. Chen, *Small* **2024**, *20*, 2305562.
[28] Xiao-Du Liang, Na Tian, Sheng-Nan Hu, Zhi-You Zhou, Shi-Gang Sun, *Mater. Rep. Energy* **2023**, *3*, 2666-9358.
[29] Y. H. Wang, W. J. Jiang, W. Yao, Z. L. Liu, Z. Liu, Y. Yang, L. Z. Gao, *Rare Met.* **2021**, *40*, 2327-2353.
[30] N. S. Shaikh, J. S. Shaikh, V. Marquez, S. C. Pathan, S. S. Mali, J. V. Patil, C. Hong, P. Kanjanaboos, O. Fontaine, A. Tiwari, S. Praserthdam, P. Praserthdam, *Mater. Today Sustain.* **2023**, *22*, 100384.
[31] Y. C. Yao, W. H. Zhuang, R. Z. Li, K. Dong, Y. L. Luo, X. He, S. J. Sun, S. Alfaifi, X. P. Sun, W. C. Hu, *ChemComm.* **2023**, *59*, 9017-9028.
[32] B. Avila-Bolívar, V. Montiel, J. Solla-Gullón, *ChemElectroChem* **2022**, *9*, e202200272.
[33] P. Lamagni, M. Miola, J. Catalano, M. S. Hvid, M. A. H. Mamakhel, M. Christensen, M. R. Madsen, H. S. Jeppesen, X. M. Hu, K. Daasbjerg, T. Skrydstrup, N. Lock, *Adv. Funct. Mater.* **2020**, *30*, 1910408.
[34] F. Li, G. H. Gu, C. Choi, P. Kolla, S. Hong, T. S. Wu, Y. L. Soo, J. Masa, S. Mukerjee, Y. S. Jung, J. S. Qiu, Z. Y. Sun, *App. Cat. B* **2020**, *277*, 119241.
[35] J. J. Bei, R. Zhang, Z. D. Chen, W. X. Lv, W. Wang, *Int. J. Electrochem. Sci.* **2017**, *12*, 2365-2375.
[36] X. X. Yang, P. L. Deng, D. Y. Liu, S. Zhao, D. Li, H. Wu, Y. M. Ma, B. Y. Xia, M. T. Li, C. H. Xiao, S. J. Ding, *J. Mater. Chem. A* **2020**, *8*, 2472-2480.
[37] C. S. Cao, D. D. Ma, J. F. Gu, X. Y. Xie, G. Zeng, X. F. Li, S. G. Han, Q. L. Zhu, X. T. Wu, Q. Xu, *Angew. Chem. Int. Ed.* **2020**, *59*, 15014-15020.
[38] D. Yao, C. Tang, A. Vasileff, X. Zhi, Y. Jiao, S.-Z. Qiao, *Angew. Chem. Int. Ed.* **2021**, *60*, 18178-18184.
[39] Z. Li, J. Y. Miao, W. Hu, Y. N. Liu, M. Li, M. L. Zhao, J. P. Liu, L. Xiao, *ChemComm.* **2023**, *59*, 5627-5630.
[40] J. H. Koh, D. H. Won, T. Eom, N.-K. Kim, K. D. Jung, H. Kim, Y. J. Hwang, B. K. Min, *ACS Catal.* **2017**, *7*, 5071-5077.
[41] C. Q. Zhu, Q. N. Wang, C. Wu, *J. CO_2 Util.* **2020**, *36*, 96-104.
[42] G. X. Piao, S. H. Yoon, D. S. Han, H. Park, *ChemSusChem* **2020**, *13*, 698-706.
[43] Y. Tian, D. Li, J. Wu, J. Liu, C. Li, G. H. Liu, D. H. Chen, Y. J. Feng, *J. CO_2 Util.* **2021**, *43*, 101360.
[44] M. Y. Fan, S. Prabhudev, S. Garbarino, J. L. Qiao, G. A. Botton, D. A. Harrington, A. C. Tavares, D. Guay, *Appl. Catal. B* **2020**, *274*, 119031.
[45] D. Ewis, M. Arsalan, M. Khaled, D. Pant, M. M. Ba-Abbad, A. Amhamed, M. H. El-Naas, *Sep. Purif. Technol.* **2023**, *316*, 123811.

[46] P. L. Deng, H. M. Wang, R. J. Qi, J. X. Zhu, S. H. Chen, F. Yang, L. Zhou, K. Qi, H. F. Liu, B. Y. Xia, *ACS Catal.* **2020**, *10*, 743-750.

[47] Y. T. Wang, Y. H. Li, J. Z. Liu, C. X. Dong, C. Q. Xiao, L. Cheng, H. L. Jiang, H. Jiang, C. Z. Li, *Angew. Chem. Int. Ed.* **2021**, *60*, 7681-7685.

[48] S. F. Tang, X. L. Lu, C. Zhang, Z. W. Wei, R. Si, T. B. Lu, *Sci. Bull.* **2021**, *66*, 1533-1541.

[49] S. Van Daele, L. Hintjens, S. Hoekx, B. Bohlen, S. Neukermans, N. Daems, J. Hereijgers, T. Breugelmans, *Appl. Catal. B* **2024**, *341*,123345.

[50] C. Nayak, V. Bhasin, K. K. Halankar, S. Banerjee, A. Bute, S. N. Jha, D. Bhattacharyya, *J. Electroanal. Chem.* **2024**, *969*, 118536.

The table of contents entry should be 50–60 words long and should be written in the present tense. The text should be different from the abstract text.

ToC figure ((Please choose one size: 55 mm broad × 50 mm high **or** 110 mm broad × 20 mm high. Please do not use any other dimensions))